



1 **Assessing snow extent data sets over North America to inform trace gas retrievals from**  
2 **solar backscatter**

3 Matthew J. Cooper<sup>1</sup>, Randall V. Martin<sup>1,2</sup>, Alexei I. Lyapustin<sup>3</sup>, and Chris A. McLinden<sup>4</sup>

4 1. Department of Physics and Atmospheric Science, Dalhousie University, Halifax, Nova Scotia,  
5 Canada.

6 2. Harvard-Smithsonian Center for Astrophysics, Cambridge, Massachusetts, USA

7 3. NASA Goddard Space Flight Center, Greenbelt, MD, USA

8 4. Air Quality Research Division, Environment and Climate Change Canada, Toronto, Ontario,  
9 Canada

10 **Abstract**

11 Accurate representation of surface reflectivity is essential to tropospheric trace gas retrievals  
12 from solar backscatter observations. Surface snow cover presents a significant challenge due to  
13 its variability; however, the high reflectance of snow is advantageous for trace gas retrievals. We  
14 first examine the implications of surface snow on retrievals from the upcoming TEMPO  
15 geostationary instrument for North America. We use a radiative transfer model to examine how  
16 an increase in surface reflectivity due to snow cover changes the sensitivity of satellite retrievals  
17 to NO<sub>2</sub> in the lower troposphere. We find that a substantial fraction (>50%) of the TEMPO field  
18 of regard can be snow covered in January, and that the average sensitivity to the tropospheric  
19 NO<sub>2</sub> column substantially increases (doubles) when the surface is snow covered.

20 We then evaluate seven existing satellite-derived or reanalysis snow extent products against  
21 ground station observations over North America to assess their capability of informing surface  
22 conditions for TEMPO retrievals. The Interactive Multisensor Snow and Ice Mapping System  
23 (IMS) had the best agreement with ground observations (accuracy=93%, precision=87%,  
24 recall=83%,  $F=85\%$ ). Multiangle Implementation of Atmospheric Correction (MAIAC)  
25 retrievals of MODIS observed radiances had high precision (90% for Aqua and Terra), but  
26 underestimated the presence of snow (recall=74% for Aqua, 75% for Terra). MAIAC generally  
27 outperforms the standard MODIS products (precision=51%, recall=43% for Aqua;  
28 precision=69%, recall=45% for Terra). The Near-real-time Ice and Snow Extent (NISE) product



29 had good precision (83%) but missed a significant number of snow covered pixels (recall=45%).  
30 The Canadian Meteorological Centre (CMC) Daily Snow Depth Analysis Data set had strong  
31 performance metrics (accuracy=91%, precision=79%, recall=82%,  $F=81\%$ ). We use the  $F$  score,  
32 which balances precision and recall, to determine overall product performance ( $F = 85\%$ ,  
33 82(82)%, 81%, 58%, 46(54)% for IMS, MAIAC Aqua(Terra), CMC, NISE, MODIS  
34 Aqua(Terra) respectively) for providing snow cover information for TEMPO retrievals from  
35 solar backscatter observations.

36

## 37 1. Introduction

38 Satellite observations of solar backscatter are widely used as a source of information on  
39 atmospheric trace gases (Richter and Wagner, 2011). These observations have provided valuable  
40 information on vertical column densities of  $O_3$ ,  $NO_2$ ,  $SO_2$ ,  $CO$ ,  $HCHO$ ,  $CH_4$  and other important  
41 trace gases in the troposphere (Fishman et al., 2008). Satellite observations of trace gases have  
42 been used to assess air quality (Duncan et al., 2014; Martin, 2008) and to gain insight into  
43 atmospheric processes including emissions (Streets et al., 2013), lifetimes (Beirle et al., 2011;  
44 Fioletov et al., 2015; de Foy et al., 2015; Valin et al., 2013), and deposition (Geddes and Martin,  
45 2017; Nowlan et al., 2014). The utility of these observations is dependent on their quality, and  
46 thus ensuring retrieval accuracy is essential.

47 Previous studies have found that retrieved  $NO_2$  vertical column densities are highly  
48 sensitive to errors in assumed surface reflectance (Boersma et al., 2004; Lamsal et al., 2017;  
49 Martin et al., 2002). Much of this error sensitivity results from observation sensitivity to trace  
50 gases in the lower troposphere. The observation sensitivity is accounted for in the air mass factor  
51 (AMF) conversion of observed line-of-sight “slant columns” to vertical column densities.  
52 Uncertainties in surface reflectance are a significant contributor to AMF uncertainty.

53 Existing reflectivity climatologies (e.g. Kleipool et al., 2008; Koelemeijer et al., 2003;  
54 Liang et al., 2002; Herman and Celarier, 1997) do not represent snow cover well, since the  
55 statistical methods to exclude reflective clouds from the climatologies also exclude variable  
56 snow cover; Therefore, snow cover is particularly challenging to retrievals. Misrepresenting  
57 surface snow cover can lead to large errors (20-50%) in retrieved  $NO_2$  columns over broad



58 regions with seasonal snow cover (O’Byrne et al., 2010). For this reason, observations over snow  
59 are often omitted to avoid potential errors. This limits the ability of satellite retrieved data sets to  
60 offer adequate temporal and spatial sampling in winter months. Additionally, observation  
61 sensitivity to the lower troposphere is larger and has less dependence on *a priori* NO<sub>2</sub> profiles  
62 over highly reflective surfaces such as snow (Lorente et al., 2017; O’Byrne et al., 2010); Thus,  
63 omitting snow-covered scenes means omitting the observations with the greatest sensitivity to  
64 the lower troposphere. This could be remedied by using a product that would allow for snow  
65 cover identification to be done with confidence.

66 Several data products provide information on snow extent using surface station  
67 observations, satellite observed radiances, or visible imagery. Previous evaluations have found it  
68 difficult to determine which of these products is definitively the best, partly due to differences in  
69 resolution. Most products are more consistent during the winter months when persistent, deep  
70 snow is present (Frei et al., 2012; Frei and Lee, 2010). However, disagreements are common  
71 during accumulation and melting seasons, over mountains, and under forest canopies. These  
72 evaluations have largely focused on local or regional snow cover, or included only cloud-free  
73 observations.

74 The upcoming geostationary Tropospheric Emissions: Monitoring of Pollution (TEMPO)  
75 satellite instrument will provide hourly observations of air quality relevant trace gases over  
76 North America at an unprecedented spatial and temporal resolution (Zoogman et al., 2017). As is  
77 the case for all nadir satellite retrievals, the quality of these observations will depend on the  
78 accuracy of the surface reflectance used in the retrieval. As a significant portion of the observed  
79 domain experiences snow cover, an accurate representation of snow cover is needed. Current  
80 plans to deal with snow cover for TEMPO are to rely on external observations.

81 In this work, we examine the importance of accurate snow identification by using a  
82 radiative transport model to evaluate how the vertical sensitivity of a satellite retrieval is  
83 impacted by surface reflectance. We then assess seven snow extent products that are expected to  
84 continue to be operational during the TEMPO mission using in situ observations across North  
85 America with the intent of determining which product is best suited for providing snow cover  
86 information for TEMPO and other future satellite retrievals.

87



88 **2. Data and Algorithms**

89 **2.1. Gridded Snow Products**

90 **2.1.1. IMS**

91 One of the most widely used sources of snow extent data is the Interactive Multisensor  
92 Snow and Ice Mapping System (IMS). IMS provides daily, near-real-time maps of snow and sea  
93 ice cover in the Northern Hemisphere at 4km resolution (Helfrich et al., 2007). The maps are  
94 produced by a trained analyst using visible imagery from a collection of geostationary and polar  
95 orbiting satellite instruments, with additional information from microwave sensors, surface  
96 observations, and models. By using multiple sources of information with different spatial  
97 resolution and temporal sampling, IMS can minimize interference from clouds.

98 **2.1.2. MODIS**

99 A second commonly used snow and ice product is derived from MODIS satellite  
100 observations from the Terra and Aqua satellites (Hall and Riggs, 2007). Terra and Aqua have  
101 sun-synchronous, near polar orbits with overpass times of 1030 and 1330 hr respectively. Snow  
102 cover is calculated using a Normalized Difference Snow Index (NDSI), which examines the  
103 difference between observed radiation at visible wavelengths (where snow is highly reflective)  
104 and short IR wavelengths (where there is little reflection from snow). Observations are made at  
105 500 m spatial resolution and aggregated to produce daily snow cover fractions on a 0.05°  
106 resolution grid. Past evaluations of the standard MODIS snow product show good agreement in  
107 cloud-free conditions but often snow is misidentified as cloud (Hall and Riggs, 2007; Yang et al.,  
108 2015).

109 The Multiangle Implementation of Atmospheric Correction (MAIAC) algorithm is also  
110 derived from MODIS observations. MAIAC retrievals uses radiances observed by the MODIS  
111 Aqua and Terra satellites to provide atmospheric and surface products including snow detection  
112 on a 1 km grid (Lyapustin et al., 2011a, 2011b, 2012). While the NDSI used by the standard  
113 MODIS product is also used by MAIAC as one of the criteria, the overall snow and cloud  
114 detection in MAIAC are different from the standard MODIS algorithm (Lyapustin et al., 2008).

115



116           **2.1.3. NISE**

117           The Near-real-time Ice and Snow Extent (NISE) provides daily updated snow cover  
118 extent information on a 25x25 km grid (Nolin et al., 2005). NISE uses microwave measurements  
119 from the Special Sensor Microwave Imager/Sounder (SSM/I) on a sun-synchronous, quasi-polar  
120 orbit to observe how microwave radiation emitted by soil is scattered by snow. Products based  
121 on microwave measurements such as NISE are known to miss wet and thin snow, as wet snow  
122 emits microwave radiation similar to soil, and thin snow does not provide sufficient scattering.

123           **2.1.4. CMC**

124           The Canadian Meteorological Centre (CMC) Daily Snow Depth Analysis Data is a  
125 statistical interpolation of snow depth measurements from 8,000 surface sites across Canada and  
126 U.S. interpolated using a snow pack model (Brasnett, 1999). Unlike the aforementioned satellite  
127 products that provide snow extent, CMC provides snow depths. Daily snow maps are produced  
128 at 25 km resolution. As it a reanalysis product, there is a time delay in availability. The CMC  
129 snow depths show good agreement with independent observations over midlatitudes and is  
130 considered an improvement over previous snow depth climatologies (Brown et al., 2003).

131           **2.2 Surface observations**

132           These snow identification products are evaluated against surface station observations  
133 from the Global Historical Climatology Network-Daily (GHCN-D) database, an amalgamation  
134 of daily climate records from over 80,000 surface stations worldwide (Menne et al., 2012a).  
135 Most observations over Canada and the United States are collected by government organizations  
136 (Environment and Climate Change Canada and NOAA National Climatic Data Center,  
137 respectively) with additional measurements from smaller observation networks. While the focus  
138 of the database is collecting temperature and precipitation measurements, many stations (1,279 in  
139 Canada, 13,932 in United States in 2015 used here) also offer snow depth measurements.

140           A subset of the surface stations included in GHCN-D may also be used in the CMC  
141 reanalysis. It is difficult to definitively know which stations are used, as CMC does not routinely  
142 archive this information. However, we estimate that only 5% of the GHCN-D stations used here  
143 are located within 0.1° of a possible CMC station, and thus GHCN-D has sufficient independent  
144 information sources to evaluate the CMC product.



145           **2.3 Radiative transfer calculations**

146           The sensitivity of satellite observations of NO<sub>2</sub> to its vertical distribution is calculated  
147 here using the LIDORT radiative transfer model (Spurr, 2002). The model is used to calculate  
148 scattering weights, which quantify the sensitivity of backscattered solar radiation to NO<sub>2</sub> at  
149 different altitudes (Martin et al., 2002; Palmer et al., 2001). The observation sensitivity to lower  
150 tropospheric NO<sub>2</sub> is represented by the air mass factor. Air mass factors for OMI satellite  
151 observations in January 2013 are calculated as a useful analog for future TEMPO observations as  
152 both instruments are spectrometers observing reflected sunlight at UV to visible wavelengths.  
153 AMFs are calculated at 440 nm, at the centre of the NO<sub>2</sub> retrieval window for OMI and TEMPO  
154 where NO<sub>2</sub> has strong absorption features. Vertical NO<sub>2</sub> profiles, and other trace gas and aerosol  
155 profiles needed for the AMF calculation shown here, are obtained from a simulation of the  
156 GEOS-Chem chemical transport model version 11-01 ([www.geos-chem.org](http://www.geos-chem.org)).

157           Figure 1 shows maps of snow-free and snow-covered reflectances used here. Snow-free  
158 surface reflectance is provided by Nadir BRDF-Adjusted reflectances from the MODIS CMG  
159 Gap-Filled Snow-Free Products (Sun et al., 2017). Reflectivities at 354 nm for snow-covered  
160 scenes are derived from OMI observations as described by O’Byrne et al. (2010). While this  
161 wavelength is different than the 440 nm wavelength used to calculate AMFs, snow reflectivity  
162 has weak spectral dependence in UV-Visible wavelengths (Feister and Grewe, 1995; O’Byrne et  
163 al., 2010). Snow can increase surface reflectance by over a factor of 10 in central North America  
164 where short vegetation is readily covered by snow.

165           **3. Methods**

166           Here we test daily snow cover products for 2015. Snow products are regridded from their  
167 native resolutions to a common 4 km grid (similar to the spatial resolution of TEMPO). A grid  
168 box is considered to be snow covered if any observations within that box are snow covered.  
169 MAIAC, NISE, and IMS give only a yes/no flag for presence of snow. MODIS products provide  
170 a pixel snow fraction, and we consider any pixels with nonzero snow fractions as snow covered.  
171 Any CMC grid box with nonzero snow depth is considered snow covered.

172           GHCN-D surface measurements are used as the ground “truth” for evaluating the satellite  
173 and reanalysis snow data products tested here. If measurements from multiple surface data



174 networks exist in the same grid box, the most reliable source is used per the priority order given  
175 by GHCN-D. If observations from multiple surface stations within the most reliable network  
176 within a grid box disagree on the presence of snow on a given day, that day is excluded from the  
177 evaluation.

178 We assess the snow data sets using metrics that are commonly used for evaluating binary  
179 data sets (Rittger et al., 2013). These metrics are based on the possible outcomes for identifying  
180 snow: true positive (TP), true negative (TN), false positive (FP), and false negative (FN).  
181 Accuracy measures the likelihood that a grid box, with snow or without, is correctly classified:

$$Accuracy = \frac{TP + TN}{TP + TN + FP + FN} \quad (1)$$

182 Precision is the probability that a region identified as snow-covered has snow:

$$Precision = \frac{TP}{TP + FP} \quad (2)$$

183 Recall is the likelihood that snow cover is detected when present:

$$Recall = \frac{TP}{TP + FN} \quad (3)$$

184 The  $F$  score balances recall and precision to measure correct classification of snow without the  
185 influence of frequent snow-free periods, and is the metric which is most relevant for TEMPO:

$$F = 2 * \frac{precision * recall}{precision + recall} \quad (4)$$

#### 186 **4. Results**

187 We first examine the effect of surface reflectivity on retrieval sensitivity by using the  
188 LIDORT radiative transfer model to calculate NO<sub>2</sub> air mass factors for both snow-free and snow-  
189 covered scenarios over North America. We calculate air mass factors for all cloud-free (OMI  
190 cloud fraction < 20%) OMI NO<sub>2</sub> observations over North America in January 2013.

191 Figure 2 shows snow-covered and snow-free retrieval sensitivity (scattering weights) for  
192 a location in the US Midwest (42°N, 100°W) with a solar zenith angle of 65°. The mean snow-  
193 covered scattering weight is greater than the mean snow-free scattering weight throughout the  
194 troposphere, by factors of 2.2 below 5 km, 2.6 below 2 km, and 3.1 below 1 km. This shows that  
195 a satellite observation is up to three times as sensitive to NO<sub>2</sub> in the boundary layer in the



196 presence of snow, due to the increased absorption by NO<sub>2</sub> in the lower troposphere when the  
197 surface reflects more sunlight.

198 Figure 3 shows the distribution of AMF values over the TEMPO field of regard with and  
199 without reflectance from snow. The snow-free AMF distribution is unimodal with a median of  
200 1.2. Allowing for the presence of snow introduces a second mode with a median of 3.0. Mean  
201 AMFs increase by a factor 2.0 in the presence of snow, indicating a doubling in the sensitivity to  
202 tropospheric NO<sub>2</sub> over snow covered surfaces across North America. The impact is larger over  
203 polluted regions, as mean AMFs increase by a factor of 2.2 in regions where NO<sub>2</sub> columns  
204 exceed  $1 \times 10^{15}$  molec/cm<sup>2</sup>. Maps of AMF with and without snow cover for January 2013 show  
205 that AMF values increase over 69% of the land surface within the TEMPO domain.

206 We next examine the snow datasets to identify the one most suited for the TEMPO  
207 retrieval algorithm. Figure 4 shows the spatial distribution of false positives and false negatives  
208 in the data sets. In all data sets, both false positives and negatives are most frequent over  
209 mountainous regions, particularly in the Rocky Mountain region, consistent with previous  
210 validation studies (Chen et al., 2012, 2014; Frei et al., 2012; Frei and Lee, 2010). These errors  
211 are often attributed to differences in representativeness, as snow cover in mountain regions is  
212 often spatially inhomogeneous, and thus *in situ* measurements may not be representative of the  
213 pixel. A slight increase in the number of false positives in IMS over prairie regions may result  
214 from crop regions with high snow-free albedos being mistaken for snow in visible imagery  
215 (Chen et al., 2012; Yang et al., 2015). NISE, MODIS Aqua, and MODIS Terra have more false  
216 negatives overall, especially in the Great Lakes and New England regions. False positives are  
217 less frequent than false negatives in all data sets. IMS and CMC have the lowest frequency of  
218 false negatives. NISE and MAIAC have the lowest frequency of false positives.

219 Figure 5 shows the metrics used to evaluate data set performance. Table 1 summarizes  
220 these results. All data sets have high accuracy numbers, owing largely to a high number of true  
221 negatives during the summer months. MODIS Aqua and Terra have low recall and *F* scores.  
222 When only observations with MODIS cloud fractions less than 20% are used, MODIS has better  
223 agreement with the ground stations (*F* statistic increases from 0.38 to 0.49 at native resolution  
224 for Aqua, 0.43 to 0.63 for Terra), however this reduces the number of usable MODIS  
225 observations by up to 60%. NISE has high precision but low recall, indicating that while areas



226 classified as snow-covered by NISE are likely correct, many snow-covered regions are missing  
227 in the data set. This is consistent with evaluations by McLinden et al. (2014) and O'Byrne et al.  
228 (2010). Although CMC, IMS, and MAIAC products show an increase in frequency of false  
229 negatives over the Rocky Mountains, they retain a high precision in this region due to frequent  
230 snow cover. While MAIAC Aqua/Terra have high accuracy and precision, lower recall values  
231 indicate that they are conservative in identifying the presence of snow. This is possibly a  
232 consequence of the method used for identifying cloud, which may incorrectly classify fresh  
233 snowfall as cloud (Lyapustin et al., 2008). Data sets were also evaluated at their native  
234 resolutions and at a common 25 km resolution (Appendix). Results are similar at each resolution  
235 with two exceptions: MODIS Aqua and Terra products perform better when regridded to coarser  
236 resolution as it reduces the number of grid boxes missing observations due to cloud, and MAIAC  
237 Aqua and Terra perform better at their native resolution than at 4km or 25 km as degrading the  
238 spatial resolution results in a loss of information.

239 For all data sets, recall is generally low in two regions: along the Pacific coastline where  
240 snow depths are relatively thin, and in the south when snow is rare and generally short lived.  
241 Thin snow is likely to be less homogenous across a pixel and more likely to be obscured by  
242 forest canopies or tall grasses, and thus is difficult to observe from satellite imagery. Short lived  
243 snow in the south is likely to be missed by satellite observations, especially since clouds are  
244 often present. However, as IMS uses multiple observations at multiple times of day in addition to  
245 incorporating ground station data, it is more likely to find snow in these cases than other satellite  
246 products (Hall et al., 2010). Overall, IMS has best agreement with *in situ* observations, with the  
247 highest accuracy, recall, and *F* statistic and relatively high precision.

248 While CMC also has strong performance metrics, it is important to consider the  
249 information source used to describe snow extent in each product. Products based on satellite  
250 observations are advantageous when assessing how surface reflectivity affects backscattered  
251 radiation observed from space. For example, thin snow, or snow obscured by tree canopies, may  
252 not affect the observed brightness from space, but would be considered snow-covered by a  
253 product based on surface observations (e.g. CMC). Also, the reflectivity of a snow-covered  
254 surface decreases over time as the snow ages (Warren and Wiscombe, 1980); This effect would  
255 not be captured by snow depth measurements. And while snow depth has been used as an



256 indicator of brightness (Arola et al., 2003), it can not account for snow aging or canopy effects.  
257 IMS is based on visible satellite imagery and thus determines snow extent based on brightness  
258 from space, which is more applicable to satellite retrievals. And while most satellite-based  
259 products rely on observations made at a single overpass time and viewing geometry, IMS has the  
260 advantage of incorporating observations from multiple satellites with differing measurement  
261 times and geometries, including both geostationary and low Earth orbits. These reasons, in  
262 addition to a strong agreement with in situ measurements and near-real-time updates, make IMS  
263 best suited for informing TEMPO retrievals.

## 264 5. Conclusion

265 An accurate representation of snow cover is essential to ensuring satellite retrieval  
266 accuracy, including those from TEMPO. Radiative transfer model calculations indicate that NO<sub>2</sub>  
267 retrievals over reflective snow-covered surfaces are more than twice as sensitive to NO<sub>2</sub> in the  
268 boundary layer than over snow-free surfaces, with the greatest increases in sensitivity occurring  
269 over polluted regions. This makes snow an attractive surface over which to observe tropospheric  
270 NO<sub>2</sub>. However, the lack of confidence in snow identification has previously led many retrieval  
271 procedures to omit observations over snow. Increasing this confidence such that these  
272 observations could be included would not only improve spatial and temporal sampling, but also  
273 allow the inclusion of observations with higher quality information on the lower troposphere.

274 We evaluated seven snow extent data sets to determine their usefulness for informing  
275 satellite retrievals of trace gas from solar backscatter observations. All products were more likely  
276 to misidentify snow over mountains or where snow cover is thin or short lived. IMS had the best  
277 agreement with *in situ* observations ( $F=0.85$ ), and as a satellite based, operational, daily updated  
278 product, it is well suited for informing TEMPO satellite retrievals. The low recall value (0.45)  
279 for NISE indicated that a significant number of snow covered pixels are missed. The standard  
280 MODIS products showed medium precision and low recall owing to cloud contamination. The  
281 MAIAC products had the highest precision (0.90 for both Aqua and Terra) of those tested, but is  
282 conservative in ascribing the presence of snow (recall=0.74 for Aqua, 0.75 for Terra). CMC had  
283 strong performance metrics ( $F=0.81$ ), but as a reanalysis product based on ground observations it  
284 may not appropriately represent how a surface snow reflectivity would affect TEMPO observed  
285 radiances.



286 Future work should investigate snow reflectance products, potentially including  
287 Bidirectional Reflectance Distribution Functions (BRDF) that describe reflection at different  
288 viewing angles, that could be used when snow is detected. A retrieval algorithm that combines  
289 daily snow detection from IMS with a climatology of snow reflectance has the potential to  
290 greatly improve upon current methodologies.

291

## 292 **6. Data Availability**

293 IMS (National Ice Center, 2008), NISE (Brodzik and Stewart, 2016), MODIS Aqua (Hall  
294 and Riggs, 2016a), MODIS Terra (Hall and Riggs, 2016b), and CMC (Brown and Brasnett,  
295 2010) data are available from the NASA National Snow and Ice Data Center (<http://nsidc.org>).  
296 MAIAC Collection 6 re-processing of MODIS data started in September 2017 and is expected to  
297 be completed by the end of year. This study used MAIAC data currently available via ftp at  
298 NASA Center for Climate Simulations (NCCS):  
299 <ftp://maiac/dataportal.nccs.nasa.gov/DataRelease/>. GHCN-D data are available from the  
300 NOAA National Climatic Data Center (Menne et al., 2012b; [www.ncdn.noaa.gov](http://www.ncdn.noaa.gov)). Code for  
301 calculating scattering weights and air mass factors, and snow-covered surface reflectances used  
302 here are available at <http://fizz.phys.dal.ca/~atmos>. Snow-free surface reflectances are available  
303 at <ftp://rsftp.eos.umb.edu/data02/Gapfilled/>. The GEOS-Chem chemical transport model used  
304 here is available at [www.geos-chem.org](http://www.geos-chem.org).

## 305 **7. References**

- 306 Arola, A., Kaurola, J., Koskinen, L., Tanskanen, A., Tikkanen, T., Taalas, P., Herman, J. R.,  
307 Krotkov, N. and Fioletov, V.: A new approach to estimating the albedo for snow-covered  
308 surfaces in the satellite UV method, *J. Geophys. Res.*, 108(D17), 4531,  
309 doi:10.1029/2003JD003492, 2003.
- 310 Beirle, S., Boersma, K. F., Platt, U., Lawrence, M. G. and Wagner, T.: Megacity emissions and  
311 lifetimes of nitrogen oxides probed from space., *Science*, 333(6050), 1737–9,  
312 doi:10.1126/science.1207824, 2011.
- 313 Boersma, K. F., Eskes, H. J. and Brinkma, E. J.: Error analysis for tropospheric NO<sub>2</sub> retrieval



- 314 from space, *J. Geophys. Res. Atmos.*, 109(D4), 2004.
- 315 Brasnett, B.: A Global Analysis of Snow Depth for Numerical Weather Prediction, *J. Appl.*  
316 *Meteorol.*, 38(6), 726–740, doi:10.1175/1520-0450(1999)038<0726:AGAOSD>2.0.CO;2, 1999.
- 317 Brodzik, M. J. and Stewart, J. S.: Near-Real-Time SSM/I-SSMIS EASE-Grid Daily Global Ice  
318 Concentration and Snow Extent, Version 5, , doi:<http://dx.doi.org/10.5067/3KB2JPLFPK3R>,  
319 2016.
- 320 Brown, R. D. and Brasnett, B.: Canadian Meteorological Centre (CMC) Daily Snow Depth  
321 Analysis Data, Version 1, , doi:<http://dx.doi.org/10.5067/W9FOYWH0EQZ3>, 2010.
- 322 Brown, R. D., Brasnett, B. and Robinson, D.: Gridded North American monthly snow depth and  
323 snow water equivalent for GCM evaluation, *Atmosphere-Ocean*, 41(1), 1–14,  
324 doi:10.3137/ao.410101, 2003.
- 325 Chen, C., Lakhankar, T., Romanov, P., Helfrich, S., Powell, A. and Khanbilvardi, R.: Validation  
326 of NOAA-Interactive Multisensor Snow and Ice Mapping System (IMS) by Comparison with  
327 Ground-Based Measurements over Continental United States, *Remote Sens.*, 4(12), 1134–1145,  
328 doi:10.3390/rs4051134, 2012.
- 329 Chen, X., Jiang, L., Yang, J. and Pan, J.: Validation of ice mapping system snow cover over  
330 southern China based on Landsat Enhanced Thematic Mapper Plus imagery, *J. Appl. Remote*  
331 *Sens.*, 8(1), 84680, doi:10.1117/1.JRS.8.084680, 2014.
- 332 Duncan, B. N., Prados, A. I., Lamsal, L. N., Liu, Y., Streets, D. G., Gupta, P., Hilsenrath, E.,  
333 Kahn, R. A., Nielsen, J. E., Beyersdorf, A. J., Burton, S. P., Fiore, A. M., Fishman, J., Henze, D.  
334 K., Hostetler, C. A., Krotkov, N. A., Lee, P., Lin, M., Pawson, S., Pfister, G., Pickering, K. E.,  
335 Pierce, R. B., Yoshida, Y. and Ziemba, L. D.: Satellite data of atmospheric pollution for U.S. air  
336 quality applications: Examples of applications, summary of data end-user resources, answers to  
337 FAQs, and common mistakes to avoid, *Atmos. Environ.*, 94, 647–662,  
338 doi:10.1016/j.atmosenv.2014.05.061, 2014.
- 339 Feister, U. and Grewe, R.: Spectral albedo measurements in the UV and visible region over  
340 different types of surfaces, *Photochem. Photobiol.*, 62(4), 736–744, doi:10.1111/j.1751-  
341 1097.1995.tb08723.x, 1995.



- 342 Fioletov, V. E., McLinden, C. A., Krotkov, N. and Li, C.: Lifetimes and emissions of SO<sub>2</sub> from  
343 point sources estimated from OMI, *Geophys. Res. Lett.*, 42(6), 1969–1976,  
344 doi:10.1002/2015GL063148, 2015.
- 345 Fishman, J., Al-Saadi, J. A., Creilson, J. K., Bowman, K. W., Burrows, J. P., Richter, A.,  
346 Chance, K. V., Edwards, D. P., Martin, R. V., Morris, G. A., Pierce, R. B., Ziemke, J. R.,  
347 Schaack, T. K., Thompson, A. M., Fishman, J., Al-Saadi, J. A., Creilson, J. K., Bowman, K. W.,  
348 Burrows, J. P., Richter, A., Chance, K. V., Edwards, D. P., Martin, R. V., Morris, G. A., Pierce,  
349 R. B., Ziemke, J. R., Schaack, T. K. and Thompson, A. M.: Remote Sensing of Tropospheric  
350 Pollution from Space, *Bull. Am. Meteorol. Soc.*, 89(6), 805–821,  
351 doi:10.1175/2008BAMS2526.1, 2008.
- 352 de Foy, B., Lu, Z., Streets, D. G., Lamsal, L. N. and Duncan, B. N.: Estimates of power plant NO  
353 x emissions and lifetimes from OMI NO<sub>2</sub> satellite retrievals, *Atmos. Environ.*, 116, 1–11, 2015.
- 354 Frei, A. and Lee, S.: A comparison of optical-band based snow extent products during spring  
355 over North America, *Remote Sens. Environ.*, 114(9), 1940–1948, doi:10.1016/j.rse.2010.03.015,  
356 2010.
- 357 Frei, A., Tedesco, M., Lee, S., Foster, J., Hall, D. K., Kelly, R. and Robinson, D. A.: A review of  
358 global satellite-derived snow products, *Adv. Sp. Res.*, 50(8), 1007–1029,  
359 doi:10.1016/j.asr.2011.12.021, 2012.
- 360 Geddes, J. A. and Martin, R. V.: Global deposition of total reactive nitrogen oxides from 1996 to  
361 2014 constrained with satellite observations of NO<sub>2</sub> columns, *Atmos. Chem. Phys.*, 17(16),  
362 10071–10091, doi:10.5194/acp-17-10071-2017, 2017.
- 363 Hall, D. . and Riggs, G. A.: MODIS/Aqua Snow Cover Daily L3 Global 0.05Deg CMG, Version  
364 6, , doi:http://dx.doi.org/10.5067/MODIS/MYD10C1.006, 2016a.
- 365 Hall, D. K. and Riggs, G. A.: Accuracy assessment of the MODIS snow products, *Hydrol.*  
366 *Process.*, 21(12), 1534–1547, doi:10.1002/hyp.6715, 2007.
- 367 Hall, D. K. and Riggs, G. A.: MODIS/Terra Snow Cover Daily L3 Global 0.05Deg CMG,  
368 Version 6, , doi:http://dx.doi.org/10.5067/MODIS/MOD10C1.006, 2016b.
- 369 Hall, D. K., Fuhrmann, C. M., Perry, L. B., Riggs, G. A., Robinson, D. A. and Foster, J. L.: A



- 370 Comparison of Satellite-Derived Snow Maps with a Focus on Ephemeral Snow in North  
371 Carolina, in 67th Eastern Snow Conference, Hancock MA USA., 2010.
- 372 Helfrich, S. R., McNamara, D., Ramsay, B. H., Baldwin, T. and Kasheta, T.: Enhancements to,  
373 and forthcoming developments in the Interactive Multisensor Snow and Ice Mapping System  
374 (IMS), *Hydrol. Process.*, 21(12), 1576–1586, doi:10.1002/hyp.6720, 2007.
- 375 Herman, J. R. and Celarier, E. A.: Earth surface reflectivity climatology at 340–380 nm from  
376 TOMS data, *J. Geophys. Res. Atmos.*, 102(D23), 28003–28011, doi:10.1029/97JD02074, 1997.
- 377 Kleipool, Q. L., Dobber, M. R., de Haan, J. F. and Levelt, P. F.: Earth surface reflectance  
378 climatology from 3 years of OMI data, *J. Geophys. Res.*, 113(D18), D18308,  
379 doi:10.1029/2008JD010290, 2008.
- 380 Koelemeijer, R. B. A., de Haan, J. F. and Stammes, P.: A database of spectral surface reflectivity  
381 in the range 335–772 nm derived from 5.5 years of GOME observations, *J. Geophys. Res.*,  
382 108(D2), 4070, doi:10.1029/2002JD002429, 2003.
- 383 Lamsal, L. N., Janz, S. J., Krotkov, N. A., Pickering, K. E., Spurr, R. J. D., Kowalewski, M. G.,  
384 Loughner, C. P., Crawford, J. H., Swartz, W. H. and Herman, J. R.: High-resolution NO<sub>2</sub>  
385 observations from the Airborne Compact Atmospheric Mapper: Retrieval and validation, *J.*  
386 *Geophys. Res. Atmos.*, 122(3), 1953–1970, doi:10.1002/2016JD025483, 2017.
- 387 Liang, S., Fang, H., Chen, M., Shuey, C. J., Walthall, C., Daughtry, C., Morisette, J., Schaaf, C.  
388 and Strahler, A.: Validating MODIS land surface reflectance and albedo products: methods and  
389 preliminary results, *Remote Sens. Environ.*, 83(1–2), 149–162, doi:10.1016/S0034-  
390 4257(02)00092-5, 2002.
- 391 Lorente, A., Folkert Boersma, K., Yu, H., Dörner, S., Hilboll, A., Richter, A., Liu, M., Lamsal,  
392 L. N., Barkley, M., De Smedt, I., Van Roozendaal, M., Wang, Y., Wagner, T., Beirle, S., Lin, J.-  
393 T., Krotkov, N., Stammes, P., Wang, P., Eskes, H. J. and Krol, M.: Structural uncertainty in air  
394 mass factor calculation for NO<sub>2</sub> and HCHO satellite retrievals, *Atmos. Meas. Tech.*, 10(3), 759–  
395 782, doi:10.5194/amt-10-759-2017, 2017.
- 396 Lyapustin, A., Wang, Y. and Frey, R.: An automatic cloud mask algorithm based on time series  
397 of MODIS measurements, *J. Geophys. Res.*, 113(D16), D16207, doi:10.1029/2007JD009641,



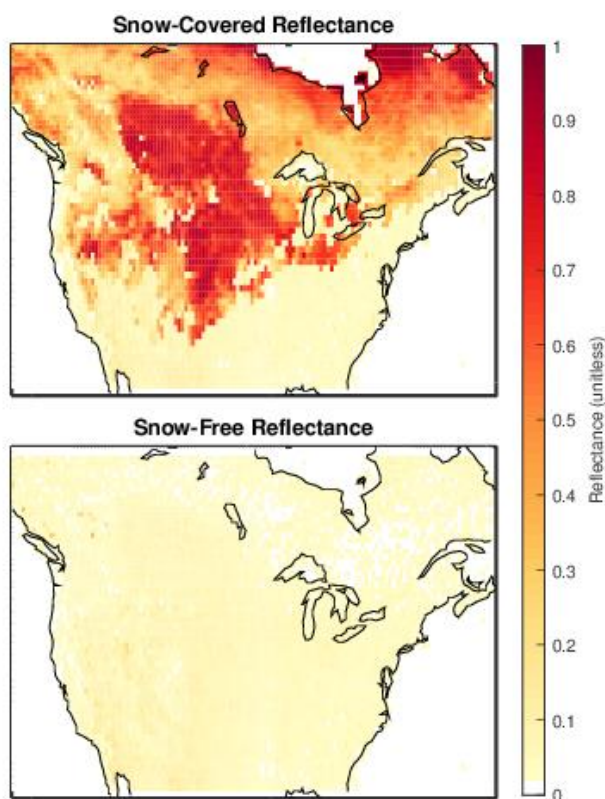
- 398 2008.
- 399 Lyapustin, A., Martonchik, J., Wang, Y., Laszlo, I. and Korkin, S.: Multiangle implementation of  
400 atmospheric correction (MAIAC): 1. Radiative transfer basis and look-up tables, *J. Geophys.*  
401 *Res.*, 116(D3), D03210, doi:10.1029/2010JD014985, 2011a.
- 402 Lyapustin, A., Wang, Y., Laszlo, I., Kahn, R., Korkin, S., Remer, L., Levy, R. and Reid, J. S.:  
403 Multiangle implementation of atmospheric correction (MAIAC): 2. Aerosol algorithm, *J.*  
404 *Geophys. Res.*, 116(D3), D03211, doi:10.1029/2010JD014986, 2011b.
- 405 Lyapustin, A. I., Wang, Y., Laszlo, I., Hilker, T., G.Hall, F., Sellers, P. J., Tucker, C. J. and  
406 Korkin, S. V.: Multi-angle implementation of atmospheric correction for MODIS (MAIAC): 3.  
407 Atmospheric correction, *Remote Sens. Environ.*, 127, 385–393, doi:10.1016/j.rse.2012.09.002,  
408 2012.
- 409 Martin, R. V., Chance, K., Jacob, D. J., Kurosu, T. P., Spurr, R. J. D., Bucsela, E., Gleason, J. F.,  
410 Palmer, P. I., Bey, I. and Fiore, A. M.: An improved retrieval of tropospheric nitrogen dioxide  
411 from GOME, *J. Geophys. Res. Atmos.*, 107(D20), 2002.
- 412 Martin, R. V.: Satellite remote sensing of surface air quality, *Atmos. Environ.*, 42(34), 7823–  
413 7843, doi:10.1016/j.atmosenv.2008.07.018, 2008.
- 414 Menne, M. J., Durre, I., Vose, R. S., Gleason, B. E., Houston, T. G., Menne, M. J., Durre, I.,  
415 Vose, R. S., Gleason, B. E. and Houston, T. G.: An Overview of the Global Historical  
416 Climatology Network-Daily Database, *J. Atmos. Ocean. Technol.*, 29(7), 897–910,  
417 doi:10.1175/JTECH-D-11-00103.1, 2012a.
- 418 Menne, M. J., Durre, I., Korzeniewski, B., McNeal, S., Thomas, K., Yin, X., Anthony, S., Ray,  
419 R., Vose, R. S., Gleason, B. E. and Houston, T. G.: Global Historical Climatology Network -  
420 Daily (GHCN-Daily), Version 3.22, , doi:http://doi.org/10.7289/V5D21VHZ, 2012b.
- 421 National Ice Center: IMS Daily Northern Hemisphere Snow and Ice Analysis at 1 km, 4 km, and  
422 24 km Resolutions, Version 1, , doi:http://dx.doi.org/10.7265/N52R3PMC, 2008.
- 423 Nolin, A., Armstrong, R. and Maslanik, J.: Near real-time SSM/I EASE-grid daily global ice  
424 concentration and snow extent, *Digit. Media*, Natl. Snow Ice Data Center, Boulder, CO, USA,  
425 2005.



- 426 Nowlan, C. R., Martin, R. V., Philip, S., Lamsal, L. N., Krotkov, N. A., Marais, E. A., Wang, S.  
427 and Zhang, Q.: Global dry deposition of nitrogen dioxide and sulfur dioxide inferred from space-  
428 based measurements, *Global Biogeochem. Cycles*, 28(10), 1025–1043,  
429 doi:10.1002/2014GB004805, 2014.
- 430 O’Byrne, G., Martin, R. V., van Donkelaar, A., Joiner, J. and Celarier, E. A.: Surface reflectivity  
431 from the Ozone Monitoring Instrument using the Moderate Resolution Imaging  
432 Spectroradiometer to eliminate clouds: Effects of snow on ultraviolet and visible trace gas  
433 retrievals, *J. Geophys. Res.*, 115(D17), D17305, doi:10.1029/2009JD013079, 2010.
- 434 Palmer, P. I., Jacob, D. J., Chance, K. and Martin, R. V: Air mass factor formulation for  
435 spectroscopic measurements from satellites’ Application to formaldehyde retrievals from the  
436 Global Ozone Monitoring Experiment, *J. Geophys. Res.*, 106(D13), 14,514-539,550, 2001.
- 437 Richter, A. and Wagner, T.: The Use of UV, Visible and Near IR Solar Back Scattered Radiation  
438 to Determine Trace Gases, pp. 67–121, Springer, Berlin, Heidelberg., 2011.
- 439 Rittger, K., Painter, T. H. and Dozier, J.: Assessment of methods for mapping snow cover from  
440 MODIS, *Adv. Water Resour.*, 51, 367–380, doi:10.1016/j.advwatres.2012.03.002, 2013.
- 441 Spurr, R. J. D.: Simultaneous derivation of intensities and weighting functions in a general  
442 pseudo-spherical discrete ordinate radiative transfer treatment, *J. Quant. Spectrosc. Radiat.*  
443 *Transf.*, 75(75), 129–175 [online] Available from: [www.elsevier.com/locate/jqsrt](http://www.elsevier.com/locate/jqsrt) (Accessed 20  
444 July 2017), 2002.
- 445 Streets, D. G., Canty, T., Carmichael, G. R., de Foy, B., Dickerson, R. R., Duncan, B. N.,  
446 Edwards, D. P., Haynes, J. A., Henze, D. K. and Houyoux, M. R.: Emissions estimation from  
447 satellite retrievals: A review of current capability, *Atmos. Environ.*, 77, 1011–1042, 2013.
- 448 Sun, Q., Wang, Z., Li, Z., Erb, A. and Schaaf, C. B.: Evaluation of the global MODIS 30 arc-  
449 second spatially and temporally complete snow-free land surface albedo and reflectance  
450 anisotropy dataset, *Int. J. Appl. Earth Obs. Geoinf.*, 58, 36–49, doi:10.1016/j.jag.2017.01.011,  
451 2017.
- 452 Valin, L. C., Russell, A. R. and Cohen, R. C.: Variations of OH radical in an urban plume  
453 inferred from NO<sub>2</sub> column measurements, *Geophys. Res. Lett.*, 40(9), 1856–1860, 2013.

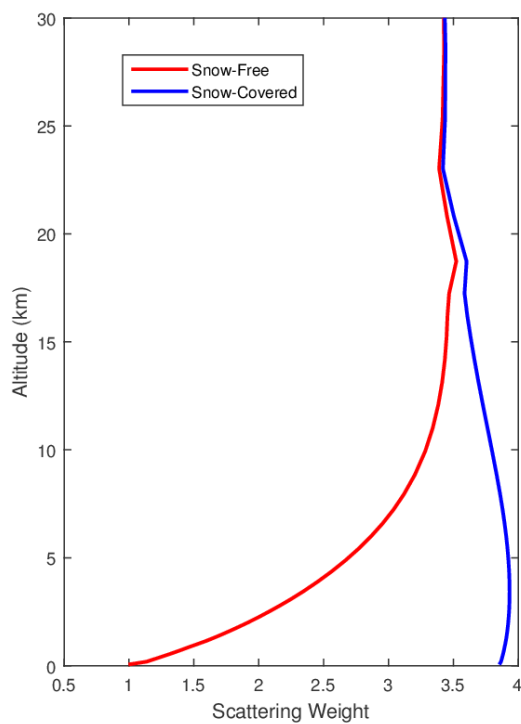


- 454 Warren, S. G. and Wiscombe, W. J.: A Model for the Spectral Albedo of Snow. II: Snow  
455 Containing Atmospheric Aerosols, *J. Atmos. Sci.*, 37(12), 2734–2745, doi:10.1175/1520-  
456 0469(1980)037<2734:AMFTSA>2.0.CO;2, 1980.
- 457 Yang, J., Jiang, L., Ménard, C. B., Luoju, K., Lemmetyinen, J. and Pulliainen, J.: Evaluation of  
458 snow products over the Tibetan Plateau, *Hydrol. Process.*, 29(15), 3247–3260,  
459 doi:10.1002/hyp.10427, 2015.
- 460 Zoogman, P., Liu, X., Suleiman, R. M., Pennington, W. F., Flittner, D. E., Al-Saadi, J. A.,  
461 Hilton, B. B., Nicks, D. K., Newchurch, M. J., Carr, J. L., Janz, S. J., Andraschko, M. R., Arola,  
462 A., Baker, B. D., Canova, B. P., Chan Miller, C., Cohen, R. C., Davis, J. E., Dussault, M. E.,  
463 Edwards, D. P., Fishman, J., Ghulam, A., González Abad, G., Grutter, M., Herman, J. R., Houck,  
464 J., Jacob, D. J., Joiner, J., Kerridge, B. J., Kim, J., Krotkov, N. A., Lamsal, L., Li, C., Lindfors,  
465 A., Martin, R. V., McElroy, C. T., McLinden, C., Natraj, V., Neil, D. O., Nowlan, C. R.,  
466 O'Sullivan, E. J., Palmer, P. I., Pierce, R. B., Pippin, M. R., Saiz-Lopez, A., Spurr, R. J. D.,  
467 Szykman, J. J., Torres, O., Veefkind, J. P., Veihelmann, B., Wang, H., Wang, J. and Chance, K.:  
468 Tropospheric emissions: Monitoring of pollution (TEMPO), *J. Quant. Spectrosc. Radiat. Transf.*,  
469 186, 17–39, doi:10.1016/j.jqsrt.2016.05.008, 2017.
- 470



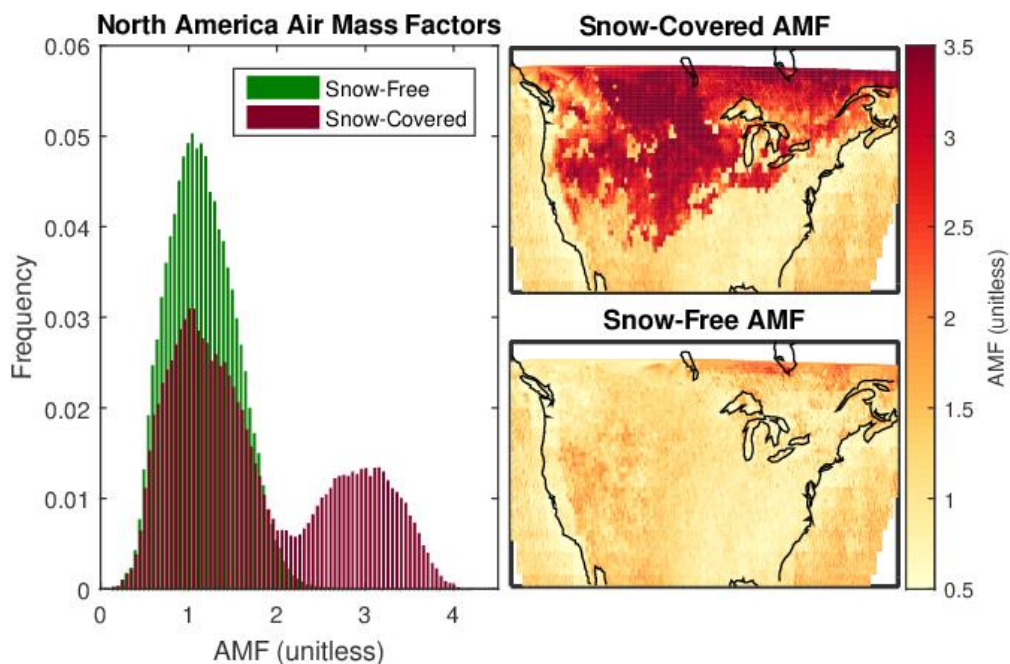
471

472 Figure 1: Surface reflectivity at visible wavelengths for snow-covered and snow-free conditions  
473 for January 2013.



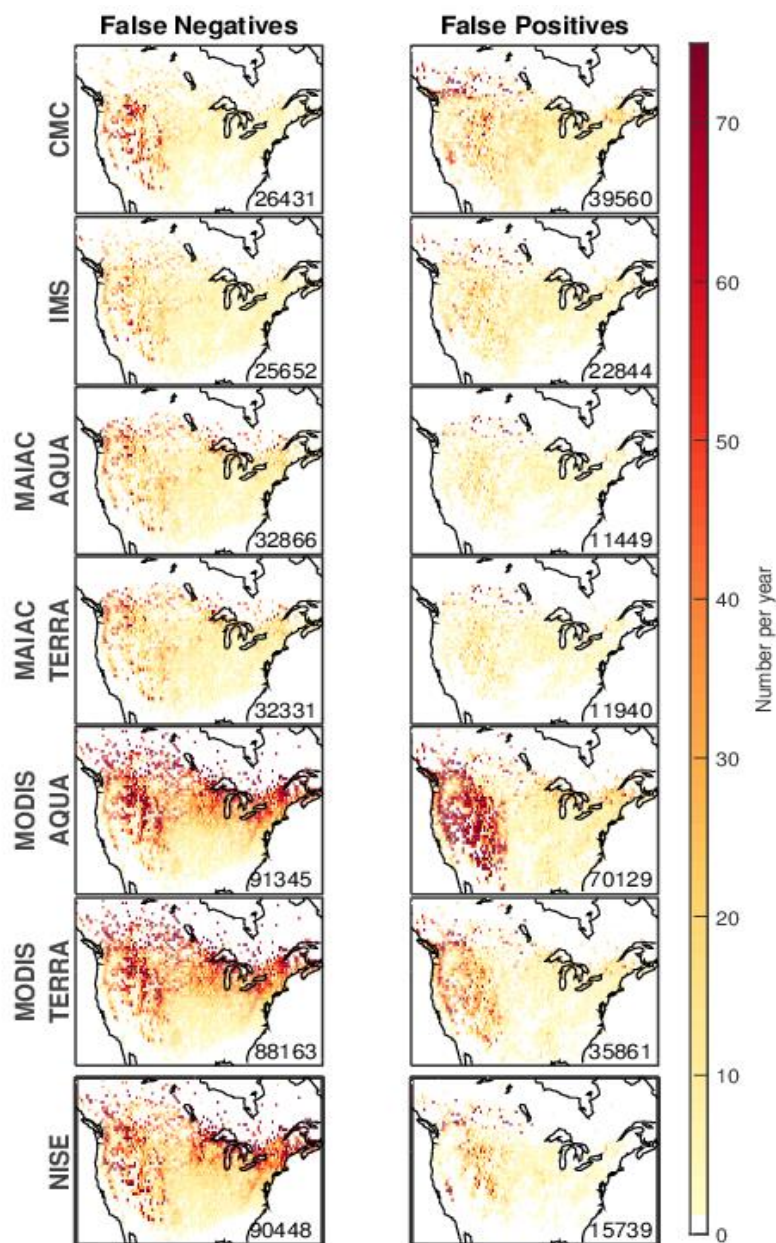
474

475 Figure 2: Observation sensitivity to NO<sub>2</sub>. Scattering weight profiles calculated for cloud-free  
476 OMI NO<sub>2</sub> retrievals, with and without surface snow cover, at 42° N, 100° W for January 2013  
477 with a solar zenith angle of 65°.



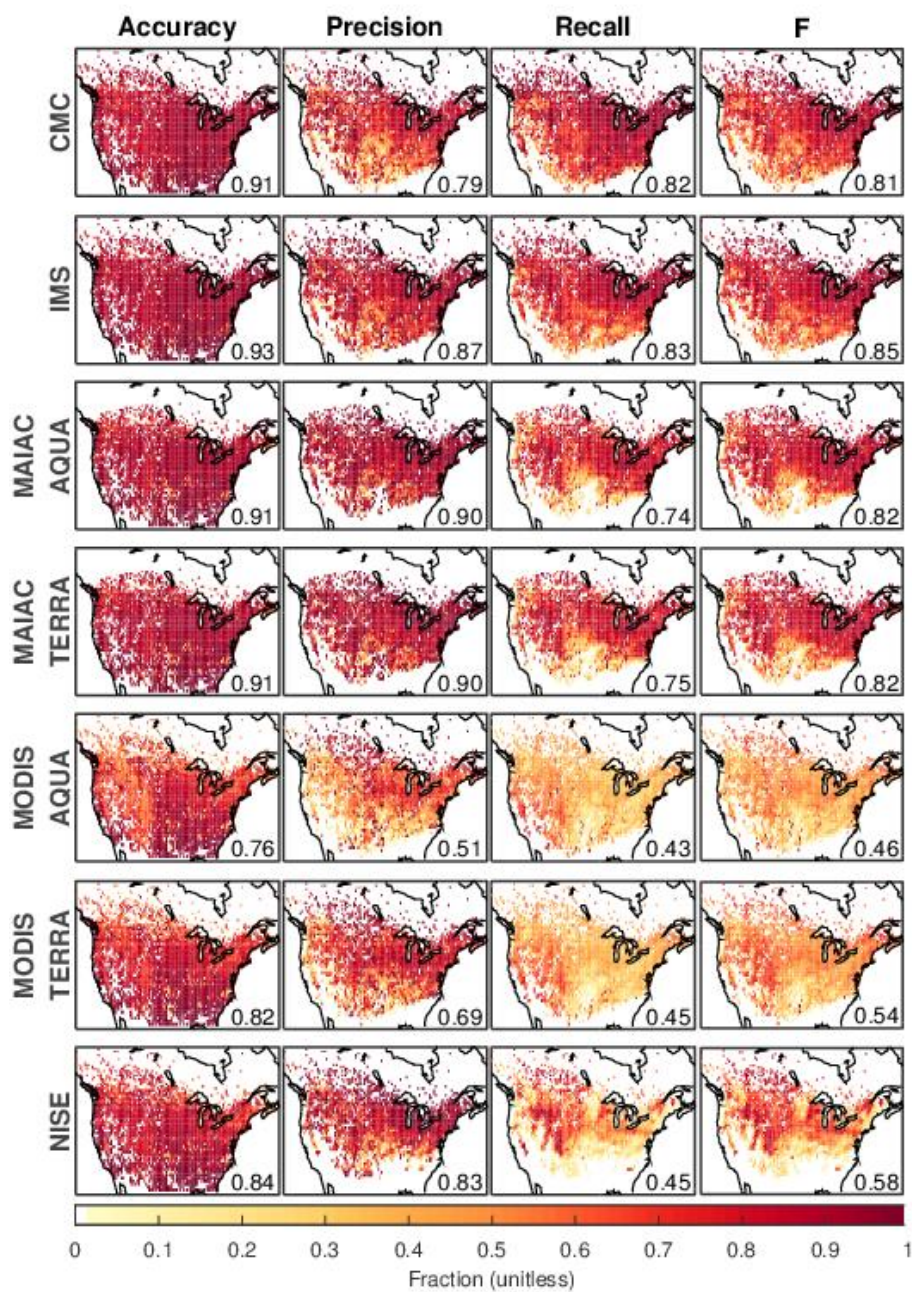
478

479 Figure 3: (Left) Distribution of Air Mass Factors (AMFs) calculated for OMI NO<sub>2</sub> retrievals over  
480 North America for January 2013, with and without surface snow cover. (Right) Maps of AMF  
481 for snow-covered and snow-free conditions.



482

483 Figure 4: Number of false positive (FP) and false negative (FN) snow attributions by the snow  
484 data sets in 2015. All data sets are evaluated at 4 km resolution. Total number of false snow  
485 attributions inset. White space indicates no ground stations present.



486

487 Figure 5: Statistical metrics to evaluate snow cover products. All data sets are gridded at 4 km

488 resolution. White space indicates no ground stations present.



	Accuracy	Precision	Recall	F
CMC	0.91	0.79	<b>0.83</b>	0.81
IMS	<b>0.93</b>	0.87	<b>0.83</b>	<b>0.85</b>
MAIAC AQUA	0.91	<b>0.90</b>	0.74	0.82
MAIAC TERRA	0.91	<b>0.90</b>	0.75	0.82
MODIS AQUA	0.76	0.51	0.43	0.46
MODIS TERRA	0.82	0.69	0.45	0.54
NISE	0.84	0.83	0.45	0.58

489 Table 1: Metrics for evaluating daily snow extent data set performance for 2015. GHCN-D

490 surface observations are used as “truth”. All products are regridded to a common 4 km

491 resolution. The highest value for each metric is shown in bold.

#### 492 Appendix

	Resolution	Accuracy	Precision	Recall	F
CMC	25 km	0.92	0.81	0.81	0.81
IMS	4 km	<b>0.93</b>	0.87	<b>0.83</b>	<b>0.85</b>
MAIAC AQUA	1 km	0.91	<b>0.91</b>	0.71	0.80
MAIAC TERRA	1 km	0.91	0.90	0.71	0.80
MODIS AQUA	0.05°	0.79	0.79	0.11	0.19
MODIS TERRA	0.05°	0.80	0.79	0.17	0.28
NISE	25 km	0.85	0.87	0.37	0.51

493 Table A1: Metrics for evaluating daily snow extent data set performance for 2015. GHCN-D

494 surface observations are used as “truth”. The highest value for each metric is shown in bold.

495

	Accuracy	Precision	Recall	F
CMC	0.92	0.81	0.80	0.80
IMS	<b>0.93</b>	0.84	<b>0.84</b>	<b>0.84</b>
MAIAC AQUA	0.87	0.69	0.69	0.69
MAIAC TERRA	0.87	0.68	0.68	0.68
MODIS AQUA	0.78	0.49	0.41	0.45
MODIS TERRA	0.83	0.68	0.43	0.53
NISE	0.85	<b>0.86</b>	0.37	0.51

496 Table A2: Metrics for evaluating daily snow extent data set performance for 2015. GHCN-D

497 surface observations are used as “truth”. All products are regridded to a common 25 km

498 resolution. The highest value for each metric is shown in bold.